Downloaded from rsta.royalsocietypublishing.org

PHILOSOPHICAL TRANSACTIONS OF THE ROYAL SOCIETY A MATHEMATICAL, PHYSICAL & ENGINEERING SCIENCES

High-Resolution Studies of Autodetachment in Negative Ions

K. R. Lykke, K. K. Murray, D. M. Neumark and W. C. Lineberger

Phil. Trans. R. Soc. Lond. A 1988 **324**, 179-196
doi: 10.1098/rsta.1988.0010

Email alerting service

Receive free email alerts when new articles cite this article - sign up in the box at the top right-hand corner of the article or click **here**

To subscribe to *Phil. Trans. R. Soc. Lond. A* go to: **http://rsta.royalsocietypublishing.org/subscriptions**

This journal is © 1988 The Royal Society

Downloaded from rsta.royalsocietypublishing.org

Phil. Trans. R. Soc. Lond. A **324**, 179–196 (1988)
Printed in Great Britain

High-resolution studies of autodetachment in negative ions

By K. R. Lykke, K. K. Murray, D. M. Neumark and W. C. Lineberger

Department of Chemistry and Biochemistry, University of Colorado, and Joint Institute for Laboratory Astrophysics, National Bureau of Standards and University of Colorado, Boulder, Colorado 80309-0440, *U.S.A.*

A review of high-resolution autodetachment spectroscopy of negative ions is given. The coaxial laser–ion-beam technique is used to probe the autodetachment dynamics of several molecular negative ions. The NH^- ($v = 1$) ion is shown to decay mainly via vibrational autodetachment, whereas CH_2CN^- detaches via rotational autodetachment. The propensity rules implied by these systems are confirmed by PtN^-, which is found to decay by both routes.

Introduction

Before 1983, C_2^- and OH^- were the only high-resolution spectroscopically studied negative ions (Herzberg & Lagerqvist 1968; Lineberger & Patterson 1972; Hotop *et al.* 1974; Jones *et al.* 1980; Schulz *et al.* 1982; Hefter *et al.* 1983; Mead *et al.* 1985). Only within the last few years has there been a flurry of high-resolution spectroscopic studies of negative ions. There are two reasons for this delay. Although negative ions are seen throughout Nature (Massey 1976), they tend to occur in relatively low abundance so that it is very difficult to do absorption spectroscopy on any but the most easily made species. Also, the outer electron in negative ions is usually bound by less than *ca.* 1 eV so that there is very little 'room' in which to have another bound electronic state. Negative-ion spectroscopy has lagged behind neutral and positive-ion spectroscopy primarily because of these two inherent problems.

The conventional spectroscopic method is absorption of a beam of light by the absorbing species. Because negative ions occur in only low concentration, the sensitivity of absorption spectroscopy has had to be increased to observe negative ions in the gas phase. A major improvement in the sensitivity of absorption spectroscopy of negative ions (and positive ions) has come from the introduction of velocity-modulated spectroscopy (Saykally 1986). The negative ions that have been observed by this technique are typically among the most abundant negative ions in a plasma (Rosenbaum *et al.* 1986; Rehfuss *et al.* 1986; Kawaguchi & Hirota 1986; Tack *et al.* 1986) (OH^-, FHF^-, NH_2^-) and are down in concentration from positive ions by only *ca.* 1–3 orders of magnitude. A very desirable feature of direct absorption spectroscopy is that any molecule, in general, will have an absorption spectrum in some spectral region. Some drawbacks to this technique include limited ion-mass selectivity and large Doppler widths.

One method for circumventing the small concentration problem is to form a beam of negative ions and detect each photon absorbed with high efficiency. This can be done if each negative ion that absorbs a photon is excited to a state above the detachment continuum, and subsequently decays by autodetachment ('autodetachment spectroscopy'). Every electron and

The Royal Society is collaborating with JSTOR to digitize, preserve, and extend access to *Philosophical Transactions of the Royal Society of London. Series A, Mathematical and Physical Sciences.* www.jstor.org

Downloaded from rsta.royalsocietypublishing.org

every neutral that is formed by this process can be detected with close to unity efficiency. Mass selectivity is another feature of this method, and by using a coaxial ion beam–laser beam, one is able to obtain greatly reduced Doppler widths. A drawback of autodetachment spectroscopy is that the upper state of the transition has to lie above the detachment threshold; no bound states can be probed by this technique.

A number of approaches have been utilized to circumvent the lack of negative-ion excited electronic states. One method that has been shown to be successful is vibrational autodetachment spectroscopy (Neumark *et al.* 1985). This involves excitation of the negative ion to a vibrationally excited state that lies above the detachment threshold. When applicable, this is a very good method for determining the structural characteristics of the ion and for obtaining detailed information on the interaction between the rotating and vibrating neutral and the detached electron. The crucial drawback to this technique is that it may not be general. The electron affinity of the neutral must lie below the vibrational level excited in the negative ion and the autodetachment lifetime must be in the range 10^{-7}–10^{-12} s for this approach to be successful.

Another method that might be general is two-photon detachment (one-photon resonant). This method has only been applied (Lineberger & Patterson 1972) in the case of C_2^-, in which both photons were the same frequency. The principle of the technique is to use a tunable laser to excite the molecular ion to an excited state (vibrational or electronic) and then detach this excited state with a high-power laser with photon frequency low enough so that it cannot detach ground-state molecules. Thus, molecules with electron affinities greater than their vibrational fundamental frequencies could be studied by this method. However, this method has not yet been demonstrated for vibrational spectroscopy.

A third method involves dipole bound states (DBS) of negative ions, states that are analogous to Rydberg states in neutral molecules. The spectroscopy of Rydberg states in neutrals has greatly increased the understanding of molecular structure (Gallas *et al.* 1985). There are an infinite number of Rydberg states in each molecule, bound by the $1/r$ potential between the positive-ion core and the electron, converging to the ionization limit of the neutral. Because there is no $1/r$ long-range potential between the neutral core and the electron in an anion, there are no Rydberg states in negative ions. However, a molecule with dipole moment greater than *ca.* 2 D† will bind an electron in the $1/r^2$ potential and produce Rydberg-type DBS (Crawford 1967; Garrett 1970, 1971, 1980, 1982; Turner 1977; Zimmerman & Brauman 1977*a*, *b*; Jackson *et al.* 1979, 1981; Mead *et al.* 1984; Lykke *et al.* 1984; Andersen *et al.* 1986, 1987; Marks *et al.* 1987). These states are weakly bound (typically less than or about 100 cm^{-1}) relative to the neutral molecule, the electron is bound in a very diffuse orbital, and the DBS is structurally similar to the neutral core, much like a Rydberg state. However, there are generally only one or two of these dipole-bound electronic states for each dipole neutral molecule, unlike the infinity of Rydberg states in each neutral molecule.

We can exploit these properties of DBS in negative-ion spectroscopy. Transitions from the ground electronic state of the negative ion to the DBS will yield autodetachment resonances in the upper, unbound rotational–vibrational levels. Analysis of this bound–quasibound transition will give structural information about both the anion ground state and the DBS, hence the neutral core. Also, because the electron is bound by the anisotropic $1/r^2$ dipole potential, the

† 1 D = 3.33×10^{-30} C m.

PHILOSOPHICAL TRANSACTIONS OF THE ROYAL SOCIETY A MATHEMATICAL, PHYSICAL & ENGINEERING SCIENCES

PHILOSOPHICAL TRANSACTIONS OF THE ROYAL SOCIETY A MATHEMATICAL, PHYSICAL & ENGINEERING SCIENCES

Downloaded from rsta.royalsocietypublishing.org

lifetime of the autodetaching resonances will give information about the interaction between a rotating–vibrating dipole and an electron. This will also help us to understand the process of autoionization in neutral molecules, where only a few systems have been studied with rotational resolution.

In this paper, we discuss three different autodetaching systems. The first one is NH^-, probed by vibrational spectroscopy. The next system discussed is CH_2CN^-, a dipole bound system studied by electronic spectroscopy. This species contains the major physical properties of DBS, but is the simplest to understand of the systems studied to date (Zimmerman & Brauman 1977*a*, *b*; Jackson *et al.* 1979, 1981; Mead *et al.* 1984; Lykke *et al.* 1984; Marks *et al.* 1987). It looks very much like a linear dipole (CCN skeleton) with perturbing hydrogens. The last system discussed is PtN^-, which is studied by electronic spectroscopy and helps to elucidate many dynamical aspects of autodetachment. However, before these systems are discussed, a brief summary of the experimental methods will be given, followed by a brief review of the autodetachment process.

Experimental

An overview of the photodetachment apparatus is presented in figure 1. The basic idea is to merge a continuous tunable laser with a mass-selected, negative-ion beam. These two beams then interact for *ca.* 30 cm and the products of photoabsorption neutrals and electrons are observed. The ion beam is formed by extracting negative ions from any one of a number of sources (see below), accelerating the ions to 2–3 keV, mass selecting with a momentum analyser, and forming a well-collimated beam with lenses and apertures. Then the ion beam is turned 90° with a transverse electric field and copropagated with the laser beam before it is turned 90° again into a Faraday cup for monitoring. Typical ion currents are between 1 pA (*ca.* 10^7 ions s^{-1}) and 10 nA (*ca.* 10^{11} ions s^{-1}). The laser beam is sent through CaF_2 brewster windows and is monitored with Fabry–Perot spectrum analysers, a λ-meter for wavelength calibration and a power meter for cross-section normalization. The typical powers available are *ca.* 10–1000 mW in a *ca.* 0.1 cm^2 beam.

The remaining ions are deflected by the second transverse electric field and those neutral species formed by detachment (or dissociation) strike a CaF_2 plate. This impact produces secondary electrons that are then detected by an electron multiplier and counted to yield the total photodestruction cross section. The electrons that are detached in the interaction region are collected by a weak solenoidal field (*ca.* 5–10 G†) and detected by another electron multiplier.

The data are taken by scanning the laser in frequency (measured with a λ-meter) while monitoring the neutrals and electrons formed as a function of laser frequency and normalizing to the ion current and laser power. The various lasers that have been utilized in this photodetachment spectrometer are home-built single-mode cw dye lasers (covering the range from *ca.* 400–1000 nm), commercial F-centre lasers (F_A(II) and F_B(II) lasers covering the range from 2.2–3.5 μm) and home-built single-mode continuous-wave (cw) F_2^+-centre lasers (covering the range 1.5–1.8 μm).

† 1 G = 10^{-4} T.

PHILOSOPHICAL TRANSACTIONS OF THE ROYAL SOCIETY A MATHEMATICAL, PHYSICAL & ENGINEERING SCIENCES

PHILOSOPHICAL TRANSACTIONS OF THE ROYAL SOCIETY A MATHEMATICAL, PHYSICAL & ENGINEERING SCIENCES

Downloaded from rsta.royalsocietypublishing.org

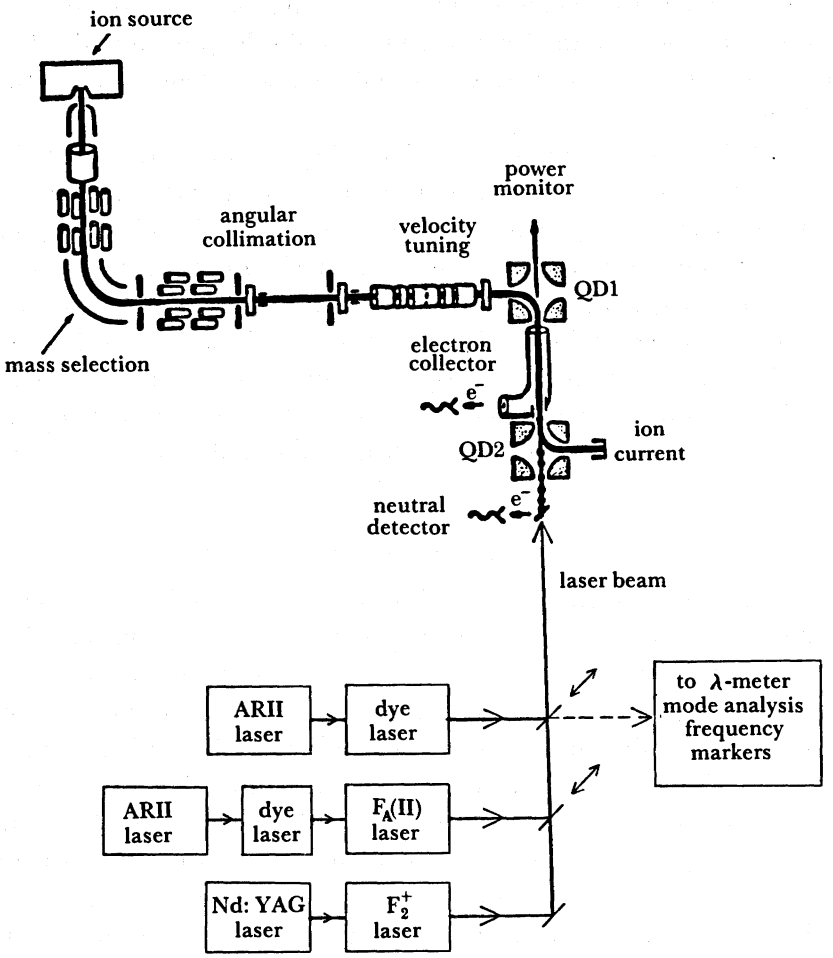

FIGURE 1. Overview of autodetachment apparatus. Note the wide selection of lasers required to cover a large portion of the spectrum from the visible to infrared.

AUTODETACHMENT PROCESSES AND RATES

Autodetachment mechanisms

Basically, the phenomenon of autodetachment (autoionization) stems from the breakdown of the Born–Oppenheimer approximation, namely, terms that couple the bound states to the continuum. From these couplings, we can calculate transition rates into the continuum via the Golden Rule (Berry 1966)

$$\text{rate} \propto \frac{2\pi}{\hbar} |\langle \psi_f | \boldsymbol{T} | \psi_i \rangle|^2 \rho$$

$$\propto \frac{2\pi}{\hbar} k^{2l+1} |\langle \psi_f | \boldsymbol{T}' | \psi_i \rangle|^2, \tag{1}$$

where $\boldsymbol{T}$ is the coupling operator, ψ_i is the wave function of the autodetaching negative ion state, ψ_f is the electron plus neutral wave function, and ρ is the density of states. The quantities k and l are the linear and angular momentum of the leaving electron and $\boldsymbol{T}'$ is the energy independent coupling operator. There are four different types of coupling operators of significance in molecular autodetachment (Berry 1966). These are: (1) configuration interaction

Downloaded from rsta.royalsocietypublishing.org

(electron–electron); (2) spin–orbit; (3) vibrational–electronic; and (4) rotational–electronic. We outline each process briefly and discuss the most important types for autodetachment.

Configuration-interaction driven autoionization arises from electron–electron repulsion and has been studied in only a few systems (Fano 1961). This coupling will only induce autodetachment if the neutral electronic state lies below the negative-ion electronic state. In the systems discussed in this paper, the negative-ion electronic state lies below the neutral electronic state, so this form of coupling is unimportant.

Spin–orbit autoionization (autodetachment) has recently been studied in several systems (Andersen *et al.* 1986, 1987; Lefebvre-Brion *et al.* 1985, 1986) and occurs when a molecular core can make a spin-orbit change to a lower state to allow the electron to leave the molecule. Spin-orbit autodetachment is unimportant for the molecules discussed here.

Rotational and vibrational autodetachment processes stem from Born–Oppenheimer breakdown (i.e. a coupling between nuclear motion and electronic motion). The coupling terms are (Hefter *et al.* 1983)

$$T' = T_{\mathrm{vib}} + T_{\mathrm{rot}}$$
$$= -\frac{\hbar^2}{2\mu}\frac{\partial}{\partial R}\bigg|_{\mathrm{el}}\frac{\partial}{\partial R}\bigg|_{\mathrm{vib}} - \frac{\hbar^2}{2\mu R^2}N|_{\mathrm{el}}\,N|_{\mathrm{rot}}. \tag{2}$$

The second term is a coupling similar (Berry 1966) to Λ-type doubling and produces coupling matrix elements proportional to $[N(N+1)]^{\frac{1}{2}}$, a coupling that should yield autodetachment rates proportional to the rotational energy. The first term in (2) can be shown (Neumark *et al.* 1985) to be proportional to $1/\epsilon_{\mathrm{if}}$ where ϵ_{if} is the nuclear energy (i.e. energy of rotation and vibration) given up in the transition. The autodetachment rate for the process primarily driven by this term would thus be proportional to $1/(\epsilon_{\mathrm{if}})^2$. Both vibrational and rotational autodetachment are important for the systems discussed in this paper.

Autodetachment line shapes

Fano (1961) has given the energy dependence of the autoionization cross section for a discrete state interacting with a continuum. The cross section

$$\sigma(\epsilon) = \sigma_{\mathrm{b}} + \frac{\sigma_{\mathrm{a}}(\epsilon+q)^2}{(\epsilon^2+1)} \tag{3}$$

depends on $\epsilon = (E-E_0)/\frac{1}{2}(h\Gamma)$, the reduced energy variable, and q, the asymmetry parameter. The quantity q^2 is the ratio of autodetachment to direct detachment. In the limit of $q \to \infty$, the resonance line approaches a lorentzian with a full width at half maximum (FWHM) given by Γ and is simply related to the lifetime of the state by the Heisenberg Uncertainty Principle.

Most molecular negative ions possess many (*ca.* 1000–10000) different initial vibration–rotation states each of which undergoes direct photodetachment with a cross section *ca.* 10^{-19} cm^2. Therefore, for the autodetachment to be observed on this background, the cross section for autodetachment must be greater than about 10^{-16} cm^2. Also, this autodetaching state cannot interact with all of the underlying continua so that $q > 100$, which fulfills the above criterion for a lorentzian. Therefore, by fitting the resonances (at least in the vibrational ground state in the autodetaching states) to lorentzians, the lifetime (and the rate) is determined.

Downloaded from rsta.royalsocietypublishing.org

Examples of negative-ion autodetachment

(a) NH^-

The only detailed example of vibrational autodetachment from a ground electronic state available at present is NH^-. The lack of other examples can in part be traced to the difficulty of finding systems whose vibrational fundamental frequencies exceed the electron affinity, and the lack of convenient, high-power sources of tunable infrared radiation. Shown in figure 2*a* is a simplified overview of the relevant NH^- and NH energy levels. The first-excited vibrational level of NH^- is unbound with respect to detachment to the lowest vibrational level of NH. Therefore, the vibration–rotation spectrum of NH^- should appear as an autodetachment spectrum riding on a small non-resonant detachment continuum. Neumark *et al.* (1985) observed transitions up to $J' \approx 13.5$ in $v' = 1$, and Al-za'al *et al.* (1986) extended these data to $J' \approx 36.5$ in $v' = 1$.

The major findings in Neumark *et al.* (1985) were a set of spectroscopic constants (which were extremely close to the calculated (Rosmus & Meyer 1978) values), and the dependence of the autodetachment rate on rotational quantum number. We will not go into any of the spectroscopic findings here but will concentrate on the autodetachment dynamics in NH^-.

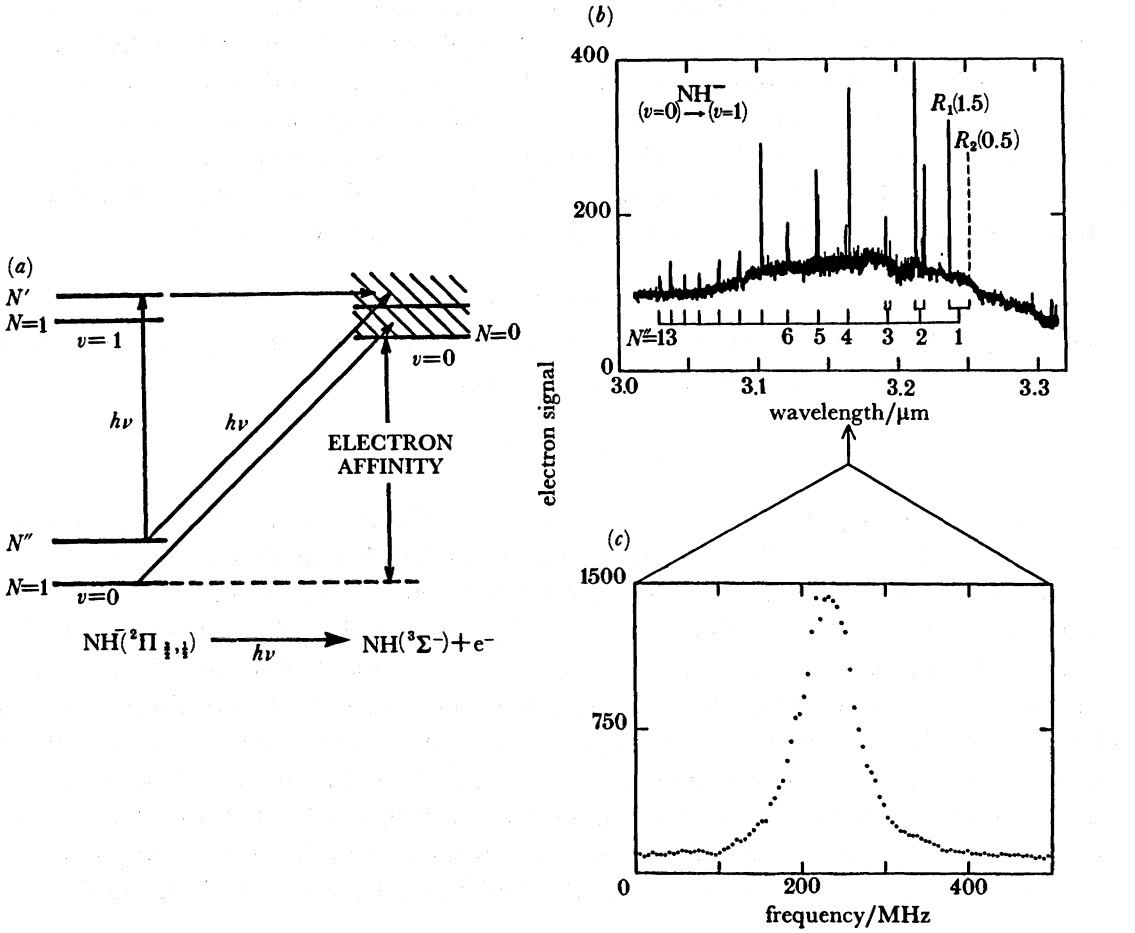

Figure 2. (*a*) Simplified energy-level diagram of the lowest vibrational levels in NH^-. (*b*) Low-resolution autodetachment spectrum of NH^- between 3.0 and 3.3 μm. (*c*) High-resolution (*ca.* 20 MHz) spectrum of one of the lines in NH^-.

Downloaded from rsta.royalsocietypublishing.org

The NH^- ion is isoelectronic with the well-studied molecule OH. Therefore, the ground electronic state is $X^2\Pi_{\frac{1}{2},\frac{3}{2}}$ and the vibrational spectrum will consist of P-, Q- and R- branches, each composed of several sub-branches (Herzberg 1950). The important point for our discussion is that there are four different fine-structure levels for each rotational level in both $v = 0$ and $v = 1$. These levels are caused by spin–orbit splitting in the $^2\Pi$ state [$^2\Pi_{\frac{1}{2}}(F_2)$ and $^2\Pi_{\frac{3}{2}}(F_1)$] and further split into Λ-doublet levels in each rotational level. The spin decouples from the molecular axis toward high J and recouples to the rotational axis to produce F_1 components ($J = N+1$) and F_2 components ($J = N-1$) instead of the case (a) components in the $^2\Pi_{\frac{3}{2}}$ and $^2\Pi_{\frac{1}{2}}$ manifolds, respectively.

A broadband scan of NH^- with the F-centre laser is shown in figure 2b with a single-mode scan shown in figure 2c (this is an expansion of *ca.* 20000 over figure 2b). This expanded view shows that the resonant part of the coupling dominates the direct photodetachment process, so that the observed line shape is lorentzian, and that the observed line widths are simply related to lifetimes. Figure 3a shows the observed linewidths of the autodetaching transitions as a function of rotational quantum number N for the upper Λ-doublet level (upper graph) and the lower Λ-doublet level (lower graph). Note the change in scale on the graphs. The resolution of this experiment is *ca.* 30 MHz and does not separate the hyperfine components, so we can only state an upper limit on linewidth of 30 MHz and thus a lower limit on the lifetime of *ca.* 5 ns.

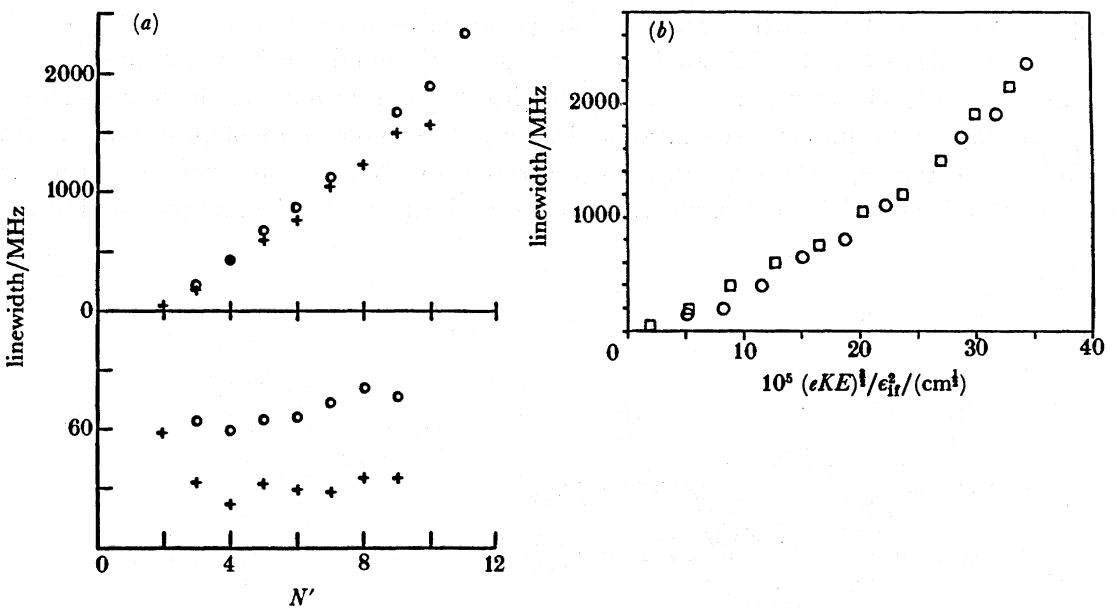

FIGURE 3. (a) Autodetachment rate (linewidth) against rotational quantum number for NH^- ($v = 1$). The linewidths were determined by fitting the resonances to lorentzians. The upper (lower) graph corresponds to the upper (lower) Λ-doublet levels. (b) Autodetachment rates for the upper Λ-doublet levels in NH^- ($v = 1$) plotted in a reduced energy release unit. If vibrational autodetachment were the only driving force, the data points would fall on a straight line in this representation. Symbols: □, F_1; ○, F_2.

The important points to notice in figure 3a are the following: (a) a relative unimportance of the autodetachment rate on spin-orbit component; (b) a drastic dependence on Λ-doublet level; and (c) an approximately linear increase of autodetachment rate as a function of the rotational quantum number for the upper Λ-doublet levels. In the following we explain these

Downloaded from rsta.royalsocietypublishing.org

phenomena with simple pictures, but first we need to see which rotational channels are open for detachment.

NH^- ($v = 1$) decays mainly via vibrational and rotational autodetachment. This should be a rapid process because of the $\Delta v = -1$ propensity rule developed by Berry (1966) for an ion and neutral with similar potential-energy curves. However, the relative energy between NH^- ($v = 1$) and $NH(v = 0)$ is not known exactly, so there is a corresponding uncertainty in the energy of the outgoing electron and even some uncertainty as to which rotational levels of NH are open channels for detachment. Neumark *et al.* (1985) observed transitions to the lowest rotational level of $NH^-(v = 1)$ (Λ-doubling was not resolved) so the electron affinity must be less than this value (*ca.* 0.374 eV), but still within the error bars quoted by Engelking & Lineberger (1976) (0.381 ± 0.014 eV). This gives the electron affinity as 0.370 ± 0.004 eV and implies that the autodetached electron from the lowest rotational level in $NH^-(v = 1)$ must have less than 0.008 eV (*ca.* 65 cm^{-1}) of energy.

NH^- approaches Hund's case (*b*) very rapidly ($J \approx 3.5$ is already in the transition to case (*b*)) so that the spin–orbit component does not have a substantial effect on the autodetachment rate; at high Js, the rotational levels approach the same energy for a given N. This transition is evident in figure 4*a*, which depicts a few representative levels for NH ($v = 0$, in the centre) and NH^- ($v = 1$, on the outside), drawn from an electron affinity of *ca.* 0.370 eV. The Λ-doublet splitting in NH^- is shown greatly exaggerated for clarity, but the very small spin splitting in NH is not shown. A few autodetachment transitions are included that display the likely channels for detachment. The possible values of angular momenta of the outgoing electron are indicated on the diagram by s($l = 0$), p($l = 1$), and d($l = 2$). The autodetachment rate for a given level will depend upon the rotational quantum numbers for the initial state (negative ion) and the final state (neutral) and l, the angular momentum of the leaving electron. In addition to the rigorous selection rules governing autodetachment, there are propensity rules for relative rates. The most important propensity is expected to be that the smallest value

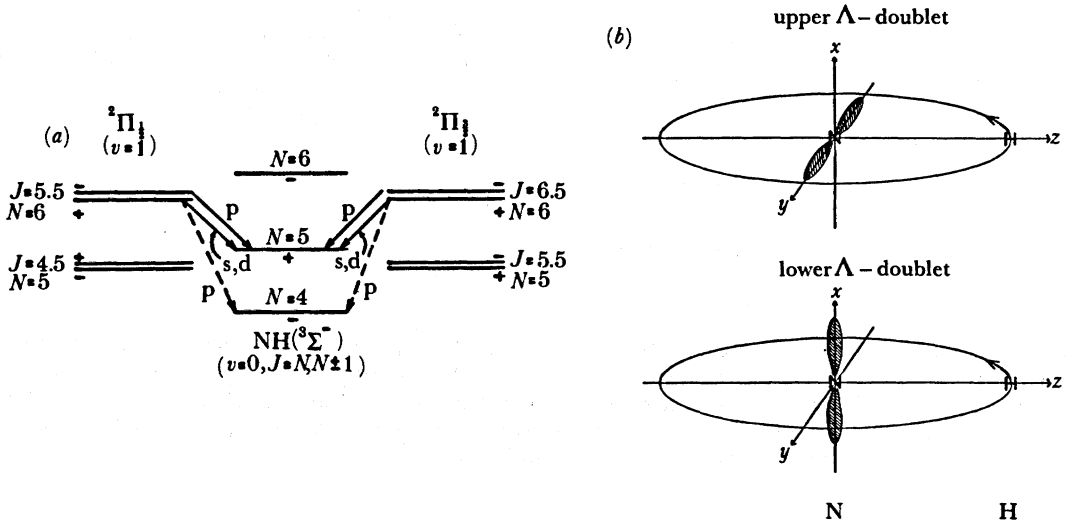

FIGURE 4. (*a*) Relevant energy levels for NH^- and NH showing some possible autodetachment transitions. (*b*) Orbital lobes involved in detachment from NH^-. Detachment occurs from the doubly occupied p-orbital localized on the N atom, almost directly on the centre of mass. The plane of rotation is the y–z plane, and the J-vector in the high rotational states lies along the x-axis.

Downloaded from rsta.royalsocietypublishing.org

of l possible for the parities of the initial and final states will be the strongest (fastest) transition. This is a result of the centrifugal barrier *ca.* $[l(l+1)]/r^2$, which the outgoing electron must conquer to leave the neutral. The next most important propensity is that rotational transitions with the smallest ΔN possible are favoured because the outgoing electron cannot exert much torque on the neutral core.

Neumark *et al.* (1985) concluded that the transitions marked with solid lines in figure 4*a* were the most probable, based upon a rough measurement of the kinetic energy of the detached electron. They could not obtain exact energies, but they could determine that both Λ-doublets of each spin–orbit manifold detached to the same level of NH. However, they observed detachment only up to $J \approx 13.5$ because of the limited user time on the borrowed laser. If one extrapolates the energy levels in figure 4*a* to higher Js, one finds that at some point the $\Delta N = -1$ channel becomes endothermic (at *ca.* $N = 29$ in NH^-) and leaves $\Delta N \geqslant -2$ as the smallest change energetically possible. This is because the difference in the rotational B, D values (e.g. $N = 35$ for NH lies *ca.* 200 cm^{-1} above $N = 36$ for NH^-). Al-za'al *et al.* (1986) reported observing up to $J \approx 36.5$ in $v = 1$ of NH^-. They report only the lower Λ-doublet because the upper Λ-level has broadened so severely that it cannot be distinguished from the underlying photodetachment continuum. If the $\Delta N = -1$ transition becomes unavailable, one should observe a narrowing of the linewidth for the upper Λ-level unless there is another factor influencing the relative detachment rates, other than low ΔN and low l. We will now attempt a brief explanation for this other factor.

NH^- and NH have the following valence molecular orbitals:

$$NH^-(^2\Pi): (2p\sigma)^2(2p\pi_{-1})(2p\pi_{+1})^2$$
$$NH(^3\Sigma^-): (2p\sigma)^2(2p\pi_{-1})(2p\pi_{+1}).$$

Therefore detachment occurs from the doubly occupied pπ orbital lobes that will tend to be oriented in different directions relative to the plane of rotation for the different Λ-levels (Andresen & Rothe 1985; Helm *et al.* 1982). The lower part of figure 4*b* corresponds to the detached p-electron lying out of the plane of rotation (lower Λ-doublet level) and the upper part of figure 4*b* corresponds to the detached p-electron (i.e. the doubly occupied orbital) lying in the plane of rotation (upper Λ-doublet level). Because the centre of mass for NH^- lies almost on the nitrogen nucleus, the p-orbital out of the plane of rotation will not feel much torque toward higher J, whereas the p-orbital in the plane of rotation will feel a large force. So rotation will tend to decouple the electron much more readily in the upper Λ-doublet state, in agreement with experiment.

Now we can make the autodetachment rate for NH^- a little more quantitative. As explained in the previous section, the autodetachment rate is given by Fermi's Golden Rule

$$W = \frac{2\pi}{\hbar} |\langle \psi_f | T | \psi_i \rangle|^2 \rho. \tag{4}$$

We calculate the vibrational autodetachment rate of the upper Λ-doublet of NH^- by following the same line of reasoning as in Neumark *et al.* (1985). However, there is a factor of k^{2l} (i.e. $(eKE)^l$) that was ignored by Neumark *et al.* This factor arises from the tunnelling motion of the leaving electron through the $l = 1$ angular-momentum barrier. Therefore, a plot of Γ (autodetachment rate) against $(eKE)^{\frac{3}{2}}/(\epsilon_{if})^2$ (figure 3*b*) should yield a straight line if vibrational autodetachment is the driving force behind detachment from the upper Λ-doublet levels.

PHILOSOPHICAL TRANSACTIONS OF THE ROYAL SOCIETY A MATHEMATICAL, PHYSICAL & ENGINEERING SCIENCES

PHILOSOPHICAL TRANSACTIONS OF THE ROYAL SOCIETY A MATHEMATICAL, PHYSICAL & ENGINEERING SCIENCES

Downloaded from rsta.royalsocietypublishing.org

Figure 3*b* shows that vibrational autodetachment is indeed the driving force behind detachment. However, there is noticeable deviation from a straight line for large releases, implying that rotational autodetachment is at work in the upper levels.

(*b*) CH_2CN^-

The CH_2CN^- ion was chosen for study because its electron affinity (*ca.* 1.5 eV) (Marks *et al.* 1986; Moran *et al.* 1987) makes the photodetachment threshold region readily accessible to cw single-mode lasers, and the CH_2CN dipole moment (*ca.* 3D) should support a weakly bound CH_2CN^- dipole-bound state. Indeed, early low-resolution photodetachment studies by Zimmerman & Brauman (1977*a*, *b*) showed unresolved structure near the photodetachment threshold, structure that was interpreted as confirming the existence of the DBS.

The total photodetachment cross section for CH_2CN^- with the dye laser in its broadband ($\Delta\nu \approx 1\,\mathrm{cm}^{-1}$) configuration is shown in figure 5*a*. This is similar to the spectrum obtained by Marks *et al.* (1986). The spectrum shows sharp structure due to autodetachment,

$$CH_2CN^- + h\nu \rightarrow (CH_2CN^-)^* \rightarrow CH_2CN + e^-, \tag{5}$$

where $(CH_2CN^-)^*$ is the dipole-bound state. This structure is superimposed on a smoothly rising background due to direct photodetachment,

$$CH_2CN^- + h\nu \rightarrow CH_2CN + e^-, \tag{6}$$

consisting of unresolved transitions to states in the (neutral + e^-) continuum. The spectrum shows two vibronic bands. The autodetachment structure in the vicinity of $12400\,\mathrm{cm}^{-1}$ is caused by transitions between the vibrationless levels of the two electronic states of CH_2CN^-, and the structure near $12000\,\mathrm{cm}^{-1}$ consists of hot-band transitions in which the ground electronic-state ions are in the $v = 2$ level of the hydrogen out-of-plane bending mode. The structure in this low-resolution spectrum represents unresolved Q-branches and is characteristic of a perpendicular electronic transition for a slightly asymmetric prolate rotor (Herzberg 1967).

A low-resolution spectrum was obtained for CD_2CN^- as well, and spectra covering the 0–0 and hot-band regions of CH_2CN^- and CD_2CN^- were taken with the laser in its single-mode configuration. Approximately 10000 transitions were recorded. A single-mode scan of a Q-branch is shown in figure 5*b*. The individual rotational transitions are clearly resolved, and the high J-transitions (at higher frequency) are considerably broader than the low J-transitions. This indicates that autodetachment is faster for the higher rotational levels of the dipole-bound state.

The observed transitions were fit to an asymmetric-top hamiltonian, including centrifugal distortion, and the complete set of constants thereby obtained for both isotopes will be listed in a future publication (Lykke *et al.* 1987). Table 1 gives A, B, and C for the $v = 0$ levels of the ground and dipole-bound states of CH_2CN^-. From these constants we see the ion is nearly a symmetric prolate rotor with $A \gg B \approx C$, so each rotational level can be labeled by J, the total rotational angular momentum, and the nearly good quantum number K, the projection of J along the ***a***-axis of the ion (the C—C≡N axis). The inertial defect Δ obtained from the rotational constants indicates that the dipole-bound state is planar and the ground state is either planar or has a very small barrier to inversion. A small inversion barrier has been inferred from a recent photoelectron-spectroscopy study of CH_2CN^- (Moran *et al.* 1987).

PHILOSOPHICAL TRANSACTIONS OF THE ROYAL SOCIETY A MATHEMATICAL, PHYSICAL & ENGINEERING SCIENCES

PHILOSOPHICAL TRANSACTIONS OF THE ROYAL SOCIETY A MATHEMATICAL, PHYSICAL & ENGINEERING SCIENCES

Downloaded from rsta.royalsocietypublishing.org

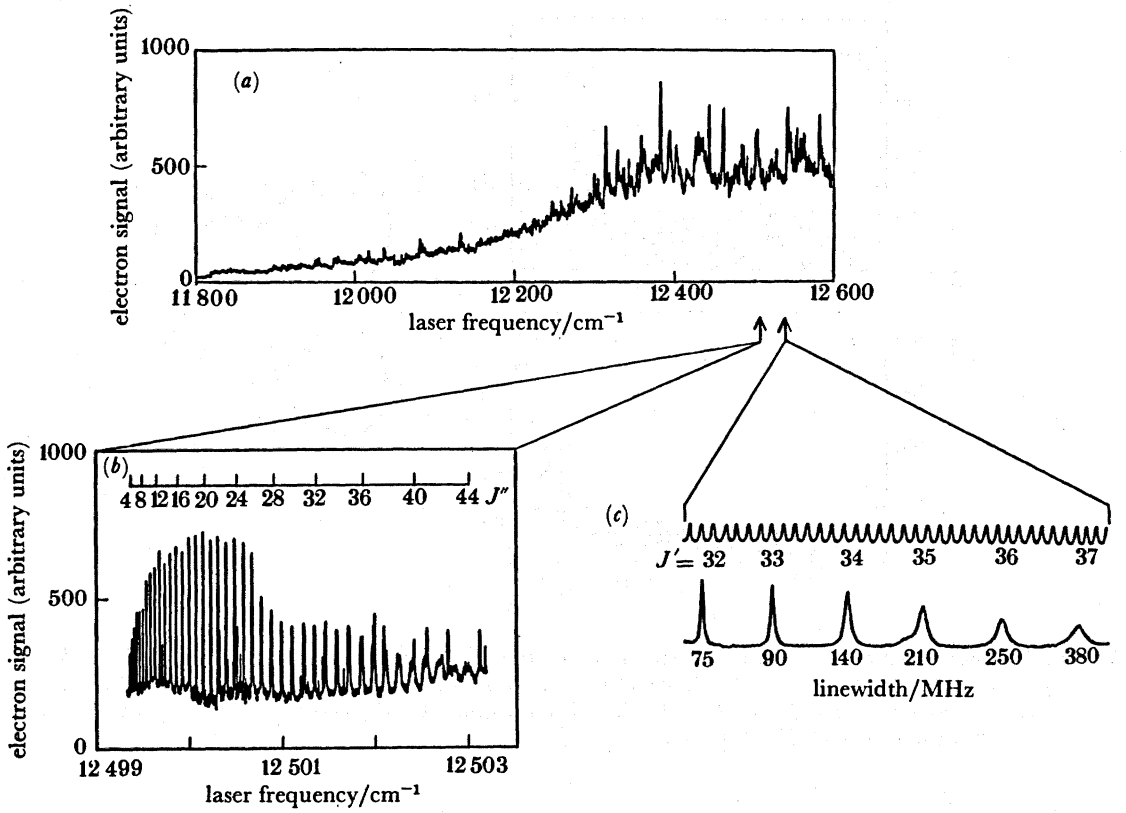

FIGURE 5. (*a*) Low-resolution (*ca.* 1 cm^{-1}) photodetachment spectrum of CH_2CN^-, showing the resonant autodetachment structure superimposed on the direct photodetachment background. (*b*) A high-resolution (*ca.* 30 MHz) expansion ($\times 200$) of the indicated portion of (*a*) ($^rQ_3$). (*c*) High-resolution scan showing the variation in linewidth as a function of J for a certain K, with *ca.* 250 MHz Fabry–Perot pips as calibration.

TABLE 1. PARTIAL LIST OF ROTATIONAL CONSTANTS FOR $v = 0$ LEVELS OF GROUND AND DIPOLE-BOUND ELECTRONIC STATES OF CH_2CN^-

	ground state	dipole-bound state
A/cm^{-1}	9.29431 (14)	9.51035 (17)
B	0.338427 (20)	0.341049 (21)
C	0.327061 (21)	0.328764 (21)
$\Delta/(u\text{Å}^2)$	−0.0827	0.0744

Finally, an analysis of the asymmetry doubling for the low K sub-bands shows that this is a $^1B_1 \leftarrow {}^1A_1$ electronic transition, and that the symmetry of the dipole-bound orbital in the upper state is a_1. Bearing in mind that this orbital is localized on the positive end of the neutral CH_2CN core, figure 6*c* qualitatively depicts the shape of the orbital for the dipole bound electron.

The linewidths of the transitions are plotted as a function of J' for different values of K' in figure 6*a* for CH_2CN^- and figure 6*b* for CD_2CN^-. Here J' and K' are the rotational quantum numbers for the dipole-bound state. The striking feature of these plots is the abrupt rise in the autodetachment rates near $J' = 33$ for CH_2CN^- and $J' = 38$ for CD_2CN^-, an onset that is independent of K'. This onset is not caused by total rotational energy because, for example,

Downloaded from rsta.royalsocietypublishing.org

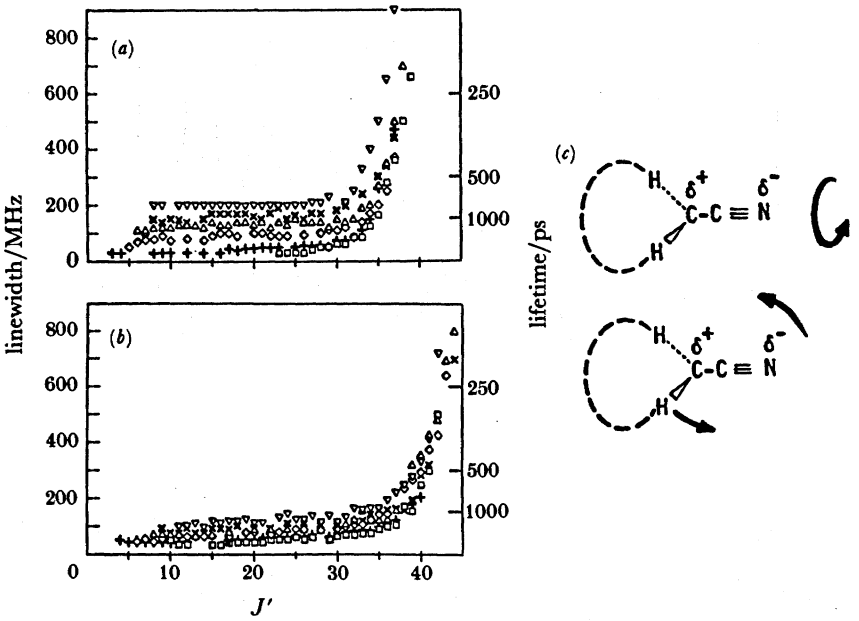

FIGURE 6. Autodetachment rate as a function of rotational quantum number for various K stacks in: (*a*) CH_2CN^- and (*b*) CD_2CN^-. (*c*) Sketch of CH_2CN^- showing the limiting rotational motions. The top (bottom) shows the motion for $J \approx K$ ($J \gg K$). The dotted line signifies the dipole-bound electron, which in actuality lies *ca.* 30 Å from the CH_2CN skeleton.

$K' = 8$ rotational levels in CH_2CN^- lie about 600 cm^{-1} above $K' = 1$ levels with the same J'.

The various mechanisms responsible for autodetachment in negative ions and autoionization in neutrals have been discussed previously. In this case, autodetachment is occurring from the vibrationless rotational levels of the dipole bound state, and rotational autodetachment should be the dominant mechanism. The rotating ion must undergo a rotational de-excitation, and the energy thereby released must eject the dipole-bound electron. In general, autodetaching transitions involving small values of ΔJ and l are favoured.

The autodetaching transitions energetically available to a given rotational level of the dipole-bound state can be determined readily once one knows the binding energy of the outermost electron in the dipole-bound state; this is the energy difference between the rotationless levels of the dipole-bound state and the ground state of neutral CH_2CN. Because the rotational levels of the dipole-bound state lying below the detachment threshold cannot autodetach, an upper limit to the binding energy can be obtained from the missing lines at low J in the spectra. For example, no transitions to $K' = 2$, $J' < 8$ are observed, placing an upper limit of *ca.* 60 cm^{-1} on the binding energy. With this limit, it can be shown that the rapid increase in the autodetachment rates in figure 6*a*, *b* coincides with an autodetaching transition of $\Delta J = -2$ or -3, $\Delta K = 0$, becoming energetically accessible. (The exact value of ΔJ depends on the binding energy, which may be lower than 60 cm^{-1}.)

For lower values of J' where the autodetachment rate is slow, autodetachment can only occur by a larger ΔJ transition, which is expected to be slow, or by a transition in which K as well as J changes. From figure 6*c*, one can qualitatively see why an autodetaching transition requiring a change in K might be very slow. Rotational autodetachment requires coupling

PHILOSOPHICAL TRANSACTIONS OF THE ROYAL SOCIETY A MATHEMATICAL, PHYSICAL & ENGINEERING SCIENCES
PHILOSOPHICAL TRANSACTIONS OF THE ROYAL SOCIETY A MATHEMATICAL, PHYSICAL & ENGINEERING SCIENCES

Downloaded from rsta.royalsocietypublishing.org

between rotational and electronic motion, and rotational angular momentum about the *a*-axis is going to be poorly coupled to the diffuse orbital of the dipole-bound electron, which is nearly cylindrically symmetric about the *a*-axis.

The strong dependence of autodetachment rate upon rotation has been observed in other cases involving dipole-bound states. In each system, abrupt rate increases can be correlated with the availability of small ΔJ, l autodetaching transitions. This type of autodetachment rate behaviour appears to be a signature of a dipole-bound state. The next system reported here, PtN^-, makes the importance of small ΔJ changes unambiguous.

(*c*) PtN^-

Molecules containing open d-shell atoms are expected to support many negative-ion electronic states. PtN^- is such a system, one that was accidentally discovered in 1972 to contain resonances. Hotop & Lineberger (1973) observed sharp resonances in the photodetachment cross section of PtN^- when they were studying threshold photodetachment of Pt^-, Au^- and Ag^-. The cold-cathode sputter source that produced the Pt^-, Au^- and Ag^- also produced copious quantities of PtN^- when N_2 was used as the sputtering gas. Because of their low-resolution detachment apparatus (*ca.* 3 cm^{-1}), they were not able to resolve rotational structure, but did set a lower limit on the lifetime of $\tau \gtrsim 5 \times 10^{-13}$ s. Because their apparatus only measured the photodestruction of the negative ion, they were unable to determine if the excited states of PtN^- decayed by autodetachment or predissociation.

Murray *et al.* (1987) recently studied the same PtN^- resonances with much higher resolution (*ca.* 30 MHz) and were able to resolve rotational structure, isotopic structure and hyperfine structure. Figure 7 shows the structure observed in their experiment and proves that the resonances observed by Hotop & Lineberger (1973) are caused by autodetachment. Figure 7*a* is the broadband photodetachment spectrum of PtN^- and is very similar to figure 9 in Hotop & Lineberger. A 'blow-up' of a small region taken with the same resolution (*ca.* 0.5 cm^{-1}) is shown in figure 7*b* and contains some rotationally resolved structure. Figure 7*c* is a high-resolution (*ca.* 30 MHz) scan of one of the resonances and shows isotopic splitting due to the three most abundant Pt isotopes. Also, the hyperfine splitting due to the ^{195}Pt nucleus appears at this resolution.

The other peaks in figure 7*a* were scanned in medium-to-high resolution but no other narrow resonances were observed. Some resonances *ca.* 10 GHz wide were found around 15400 cm^{-1}, but these were too broad and congested to analyse. A brief discussion of the analysable part of the spectrum follows.

The data obtained for the band system near 16400 cm^{-1} yielded to a spectroscopic analysis by using combination differences, followed by a least-squares fit. The resonances are from a $^1\Pi$–$^1\Sigma$ transition, followed by autodetachment from the $^1\Pi$ levels. The initial combination difference fit was hampered by the fact that Js lower than *ca.* 45 were too broad to distinguish from direct detachment and Js above *ca.* 59 were too narrow to observe (these were too long lived and did not detach in the apparatus).

The autodetachment rates against rotational quantum number are shown in figure 8. As is immediately evident, PtN^- has a much different detachment-rate dependence from the other negative ions studied to date. The autodetachment lines are very broad (rapid detachment rate) at low J and very narrow (very long lived) at high J. This is in spite of the fact that $J = 57$ lies *ca.* 450 cm^{-1} above $J = 46$. Notice also that the Q-branch has a slightly different

PHILOSOPHICAL TRANSACTIONS OF THE ROYAL SOCIETY A MATHEMATICAL, PHYSICAL & ENGINEERING SCIENCES

PHILOSOPHICAL TRANSACTIONS OF THE ROYAL SOCIETY A MATHEMATICAL, PHYSICAL & ENGINEERING SCIENCES

Downloaded from rsta.royalsocietypublishing.org

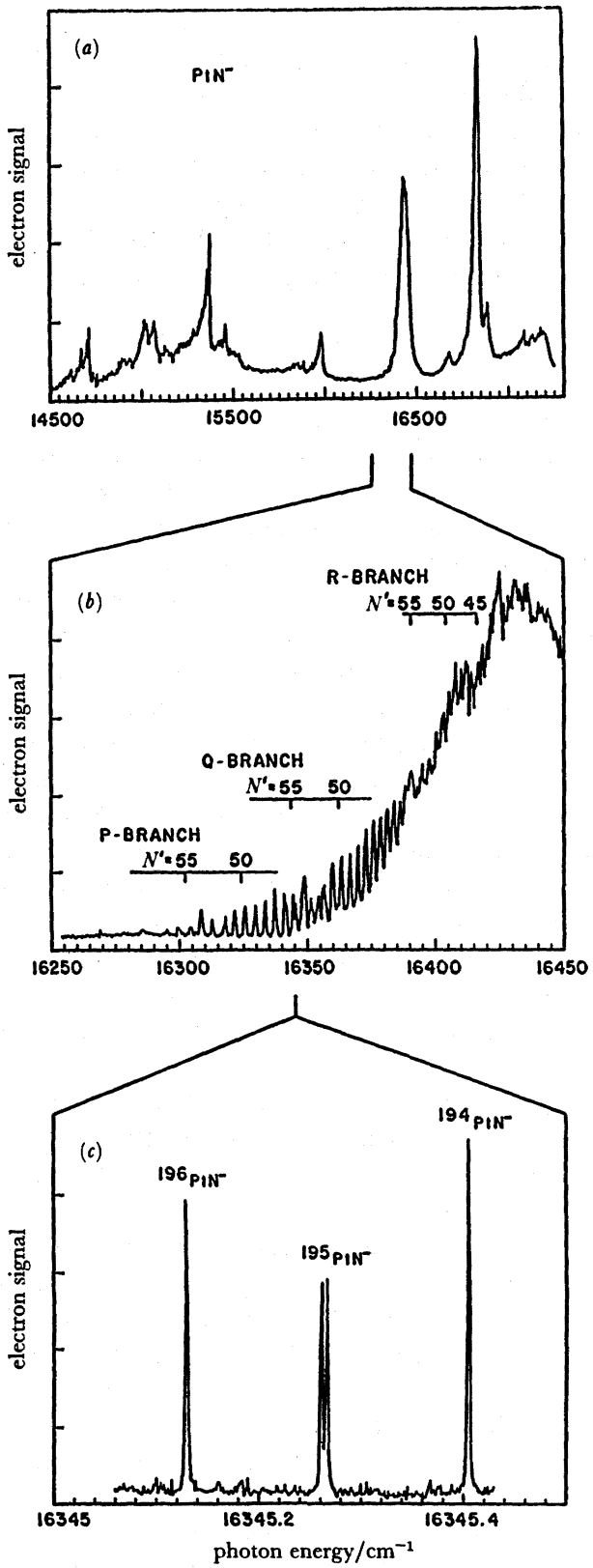

FIGURE 7. (*a*) Low-resolution photodetachment spectrum of PtN^-. (*b*) Expansion of the indicated region of (*a*), showing a hint of resolved structure. (*c*) High-resolution spectrum of one rotational line showing isotopic structure and hyperfine structure in ^{195}Pt.

PHILOSOPHICAL TRANSACTIONS OF THE ROYAL SOCIETY A MATHEMATICAL, PHYSICAL & ENGINEERING SCIENCES
PHILOSOPHICAL TRANSACTIONS OF THE ROYAL SOCIETY A MATHEMATICAL, PHYSICAL & ENGINEERING SCIENCES

Downloaded from rsta.royalsocietypublishing.org

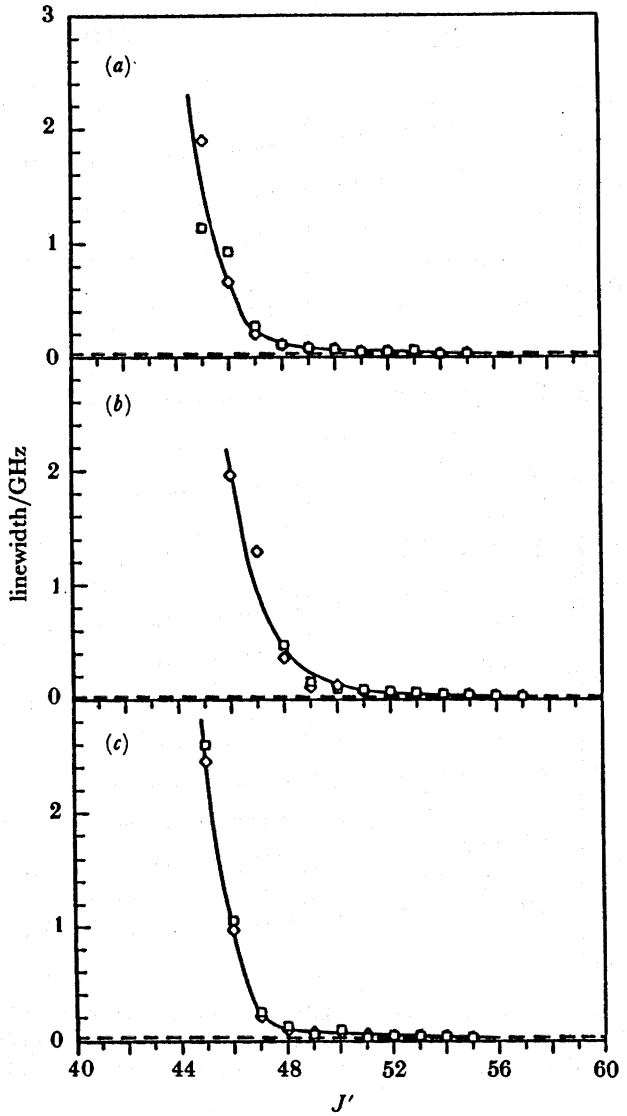

FIGURE 8. Autodetachment rate (linewidth) against rotational quantum number for various branches in PtN^-. (*a*) P-branch; (*b*) Q-branch, (*c*) R-branch.

linewidth compared to the common width observed for the corresponding P- and R-branches. This is possible because the Q-branch of a $^1\Pi$–$^1\Sigma$ transition accesses a different upper-state level than either the P- or R-branch transitions access. However, the difference in autodetachment rate for the two Λ-doublet levels in the $^1\Pi$ state is not nearly as striking as in NH^-. (The Λ-doublet levels in PtN^- differ in total energy by *ca.* 0.6 cm^{-1} at $J' = 50$.)

The need for the energy levels of the neutral PtN prompted our colleagues (D. G. Leopold, J. Ho, K. Ervin & W. C. Lineberger, unpublished results) to obtain a photoelectron spectrum of PtN^-. This yielded an electron affinity of *ca.* 16400 cm^{-1} and, when combined with the rotational constant B for PtN^-, they obtained a rotational constant for the neutral PtN, $B \approx 0.45$ cm^{-1}. From these results, Murray *et al.* (1987) were able to obtain a qualitative explanation for the autodetachment results with the help of figure 9. In the figure, a few of the rotational

Downloaded from rsta.royalsocietypublishing.org

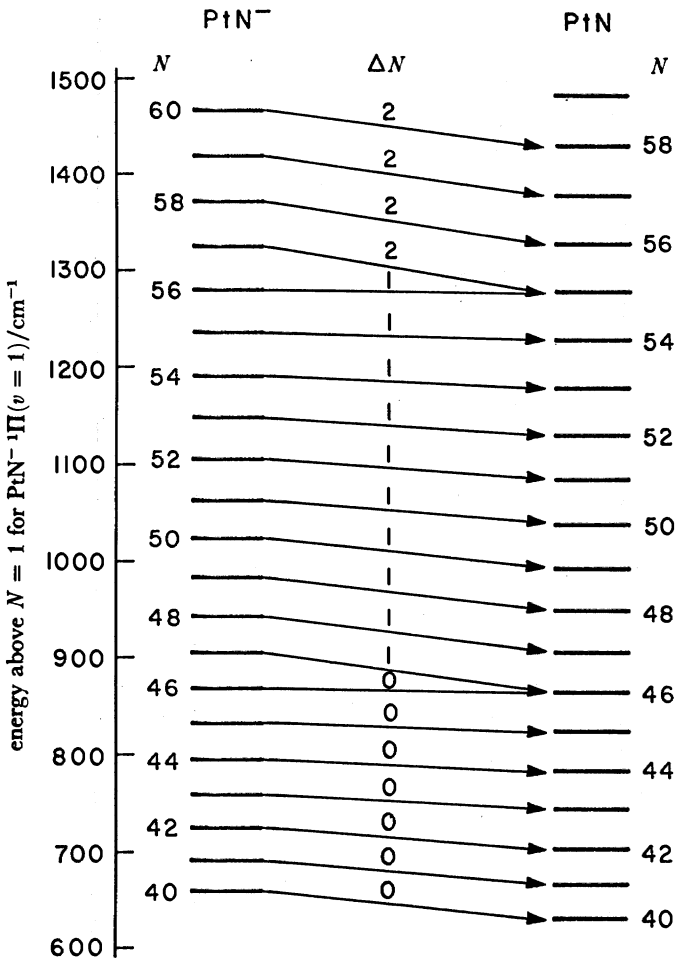

FIGURE 9. Simplified rotational energy levels for PtN^{-*} and PtN in the region of rapid linewidth variation. The relation between the PtN^- and PtN energy scales was independently determined by photoelectron spectroscopy of PtN^-. The arrows signify the fastest autodetachment channels available for each level.

levels for PtN are at the right and the levels for PtN^- are at the left. These levels are placed on the same energy scale by the photoelectron experiment, and they cannot be shifted by more than *ca.* 40 cm^{-1} with respect to each other. The transitions for the 'best' open channels are shown in the middle. The autodetachment spectroscopic results indicated that a $v' = 1 \leftarrow v'' = 0$ transition is the one observed with a term energy of *ca.* 16445 cm^{-1}. The photoelectron results indicate an electron affinity of *ca.* 16400 cm^{-1}. Therefore, the autodetachment transitions shown in figure 9 are $\Delta v = -1$ and are extremely rapid if there is a small angular-momentum barrier.

As in all of the other systems that have been studied, autodetachment from PtN^- proceeds via transitions that require the consideration of certain propensity rules. We have already stated that the preferred change in vibration is $\Delta v = -1$. Now the change in nuclear rotational motion (ΔN) should be small because the low-energy, outgoing electron cannot impart much force on the nuclei. Also, the angular momentum of the outgoing electron (l) must be small to surmount the centrifugal barrier $[l(l+1)]/r^2$. The autodetachment transition rate will also increase if the electron can leave with more energy (this will go *ca.* $(eKE)^{l+\frac{1}{2}}$, where eKE is the

Downloaded from rsta.royalsocietypublishing.org

electron kinetic energy). Taking into account these propensity rules, all of the lower Js in PtN^- can detach very rapidly via

$$\Delta v = -1,$$
$$\Delta N = 0 \quad (N = J \quad \text{for } PtN^-;\ N = J \pm \tfrac{1}{2} \quad \text{for PtN}),$$
$$l = 0, 1 \quad (\text{i.e. s- or p-waves}).$$

These channels will be open until $J \approx 45$, where the $\Delta N = 0$ channel shuts off. This will also increase the l required because the transition must follow the 'triangle rule'; the angular momentum of PtN^- (here it is J) must equal the vector sum of the angular momentum of PtN and the angular momentum of the outgoing electron. Therefore, when the $\Delta N = 0$ channel closes at $N \approx 45$, the electron must now tunnel through a large angular-momentum barrier, and the autodetachment rate decreases. At $N \approx 57$, the $\Delta N = -1$ channel shuts off, and the $\Delta N = -2$ channel is left as the fastest transition available. This means that the electron must tunnel through an even larger barrier and the negative ion excited state lives much longer than the transit time (or fluorescence time) and will not be observed. This is very much the same case as $FeO^-(B^4\Delta_{\frac{7}{2}})$ (Andersen *et al.* 1987), but with the channel openings and closings swapped; the transitions to higher Js broadened out.

Conclusions

The technique of high-resolution autodetachment spectroscopy has been shown to be very useful in understanding the dynamics involved in autodetachment. In this paper, only three representative systems were discussed, although at least seven systems have been studied. There is still much to be learned from negative-ion spectroscopy.

We thank our many colleagues in the study of negative ions. This work was supported by U.S. National Science Foundation grants PHY86-04504 and CHE83-16628.

References

Al-za'al, M., Miller, H. C. & Farley, J. W. 1986 *Chem. Phys. Lett.* **131**, 56.
Andersen, T., Lykke, K. R., Neumark, D. M. & Lineberger, W. C. 1986 *Electronic and atomic collisions* (ed. D. C. Lorents, W. E. Meyerhof & J. R. Peterson), pp. 791–798. Amsterdam: Elsevier.
Andersen, T., Lykke, K. R., Neumark, D. M. & Lineberger, W. C. 1987 *J. chem. Phys.* **86**, 1858.
Andresen, P. & Rothe, E. W. 1985 *J. chem. Phys.* **82**, 3634.
Berry, R. S. 1966 *J. chem. Phys.* **45**, 1228.
Crawford, O. H. 1967 *Proc. phys. Soc. London* **91**, 279.
Engelking, P. C. & Lineberger, W. C. 1976 *J. chem. Phys.* **65**, 4323.
Fano, U. 1961 *Phys. Rev.* **124**, 1866.
Gallas, J. A. C., Leuchs, G. & Walther, H. 1985 *Adv. atom. mol. Phys.* **20**, 413.
Garrett, W. R. 1970 *Chem. Phys. Lett.* **5**, 393.
Garrett, W. R. 1971 *Phys. Rev.* A **3**, 961.
Garrett, W. R. 1980 *J. chem. Phys.* **73**, 5721.
Garrett, W. R. 1982 *J. chem. Phys.* **77**, 3666.
Hefter, U., Mead, R. D., Schulz, P. A. & Lineberger, W. C. 1983 *Phys. Rev.* A **28**, 1429.
Helm, H., Cosby, P. C., Graff, M. M. & Moseley, J. T. 1982 *Phys. Rev.* A **25**, 304.
Herzberg, G. 1950 *Spectra of diatomic molecules*. New York: Van Nostrand.
Herzberg, G. 1967 *Electronic spectra of polyatomic molecules*. New York: Van Nostrand.
Herzberg, G. & Lagerqvist, A. 1968 *Can. J. Phys.* **46**, 2363.
Hotop, H. & Lineberger, W. C. 1973 *J. chem. Phys.* **58**, 2379.
Hotop, H., Patterson, T. A. & Lineberger, W. C. 1974 *J. chem. Phys.* **60**, 1806.

PHILOSOPHICAL TRANSACTIONS OF THE ROYAL SOCIETY A MATHEMATICAL, PHYSICAL & ENGINEERING SCIENCES
PHILOSOPHICAL TRANSACTIONS OF THE ROYAL SOCIETY A MATHEMATICAL, PHYSICAL & ENGINEERING SCIENCES

Downloaded from rsta.royalsocietypublishing.org

Jackson, R. L., Hiberty, P. C. & Brauman, J. I. 1981 *J. chem. Phys.* **74**, 3705.
Jackson, R. L., Zimmerman, A. H. & Brauman, J. I. 1979 *J. chem. Phys.* **71**, 2088.
Jones, P. L., Mead, R. D., Kohler, B. E., Rosner, S. D. & Lineberger, W. C. 1980 *J. chem. Phys.* **73**, 4419.
Kawaguchi, K. & Hirota, E. 1986 *J. chem. Phys.* **84**, 2953.
Lefebvre-Brion, H., Dehmer, P. M. & Chupka, W. A. 1986 *J. chem. Phys.* **85**, 45.
Lefebvre-Brion, H., Giusti-Suzor, A. & Raseev, G. 1985 *J. chem. Phys.* **83**, 1557.
Lineberger, W. C. & Patterson, T. A. 1972 *Chem. Phys. Lett.* **13**, 40.
Lykke, K. R., Mead, R. D. & Lineberger, W. C. 1984 *Phys. Rev. Lett.* **52**, 2221.
Lykke, K. R., Neumark, D. M., Andersen, T., Trapa, V. J. & Lineberger, W. C. 1987 *J. chem. Phys.* (In the press.)
Marks, J., Brauman, J. I., Mead, R. D., Lykke, K. R. & Lineberger, W. C. 1987 *J. chem. Phys.* (Submitted.)
Marks, J., Wetzel, D. M., Comita, P. B. & Brauman, J. I. 1986 *J. chem. Phys.* **84**, 284.
Massey, H. 1976 *Negative ions*. Cambridge University Press.
Mead, R. D., Hefter, U., Schulz, P. A. & Lineberger, W. C. 1985 *J. chem. Phys.* **82**, 1723.
Mead, R. D., Lykke, K. R., Lineberger, W. C., Marks, J. & Brauman, J. I. 1984 *J. chem. Phys.* **81**, 4883.
Moran, S., Ellis, H. B. Jr, DeFrees, D. J. & Ellison, J. B. 1987 *J. Am. chem. Soc.* (In the press.)
Murray, K. K., Lykke, K. R. & Lineberger, W. C. 1987 *Phys. Rev.* A **36**, 699.
Neumark, D. M., Lykke, K. R., Andersen, T. & Lineberger, W. C. 1985 *J. chem. Phys.* **83**, 4364.
Rehfuss, B. D., Crofton, M. W. & Oka, T. 1986 *J. chem. Phys.* **85**, 1785.
Rosenbaum, N. H., Owrutsky, J. C., Tack, L. M. & Saykally, R. J. 1986 *J. chem. Phys.* **84**, 5308.
Rosmus, P. & Meyer, W. 1978 *J. chem. Phys.* **69**, 2745.
Saykally, R. J., 1986 *Spectroscopy* **1**, 40.
Schulz, P. A., Mead, R. D., Jones, P. L. & Lineberger, W. C. 1982 *J. chem. Phys.* **77**, 1153.
Tack, L. M., Rosenbaum, N. H., Owrutsky, J. C. & Saykally, R. J. 1986 *J. chem. Phys.* **84**, 7056.
Turner, J. E. 1977 *Am. J. Phys.* **45**, 758.
Zimmerman, A. H. & Brauman, J. I. 1977*a* *J. chem. Phys.* **66**, 5823.
Zimmerman, A. H. & Brauman, J. I. 1977*b* *J. Am. chem. Soc.* **99**, 3565.

PHILOSOPHICAL TRANSACTIONS OF THE ROYAL SOCIETY A MATHEMATICAL, PHYSICAL & ENGINEERING SCIENCES

PHILOSOPHICAL TRANSACTIONS OF THE ROYAL SOCIETY A MATHEMATICAL, PHYSICAL & ENGINEERING SCIENCES